AMERICAN METEOROLOGICAL SOCIETY
AMS Journals Online

Journals   Subscribe   For Authors   Information   Online Help

Quick Search | Full Text ▾ |

Table of Contents

Related Articles

Articles Citing this Article
Google Scholar

< Previous Article   **Volume 44, Issue 5 (May 2005)**   Next Article >

Add to Favorites   Email   Download to Citation Manager   Track Citations   Glossary
Permissions

Abstract   **PDF**   **Figures**   **Tables**

Flow around a Complex Building: Experimental and Large-Eddy Simulation Comparisons

Ronald Calhoun , Frank Gouveia , Joseph Shinn , Stevens Chan , Dave Stevens , Robert Lee , and John Leone

Lawrence Livermore National Laboratory, Livermore, California

Abstract

A field program to study atmospheric releases around a complex building was performed in the summers of 1999 and 2000. The focus of this paper is to compare field data with a large-eddy simulation (LES) code to assess the ability of the LES approach to yield additional insight into atmospheric release scenarios. In particular, transient aspects of the velocity and concentration signals are studied. The simulation utilized the finite-element method with a high-fidelity representation of the complex building. Trees were represented with a canopy term in the momentum equation. Inflow and outflow conditions were used. The upwind velocity was constructed from a logarithmic law fitted to velocities obtained on two levels from a tower equipped with a 2D sonic anemometer. A number of different kinds of comparisons of the transient velocity and concentration signals are presented—direct signal versus time, spectral, Reynolds stresses, turbulent kinetic energy signals, and autocorrelations. It is concluded that the LES approach does provide additional insight, but the authors argue that the proper use of LES should include consideration of cost and may require an increased connection to field sensors; that is, higher-resolution boundary and initial conditions need to be provided to realize the full potential of LES.

Introduction

   Flow and dispersion around buildings are becoming an increasingly important problem in the atmospheric sciences. This increase in importance is due in part to the rapid urbanization of our population and the enhanced perception of threats and catastrophes that may affect urban populations. There has been a significant and steady effort to understand these problems better (e.g., Brown et al. 2001; Murakami 1993; Ramsdell and Fosmire 1998). Simulation methods have been developed and applied extensively to model problems that are meant to capture some of the effects present in larger-scale atmospheric problems (e.g., Calhoun and Street 2001; Ding et al. 2003). These efforts to understand and simulate "model" atmospheric problems have been productive because of the careful measurements that can be obtained for these domains (e.g., Snyder 1994; Lawson et al. 2000). Reynolds-averaged Navier–Stokes solutions (RANS) and large-eddy simulations (LES) have both been applied to these problems. In the following, the authors compare LES solutions with measurements taken during a field experiment. For a critical review of LES in the atmospheric sciences, see Mason (1994).

   In the summers of 1999 and 2000, an experimental program was performed of atmospheric releases using a tracer gas around a complex building. Surface energy budget stations, 2D sonic anemometers, and tracer-gas samplers were used in the study. The overall goal of the experimental program was to provide better data for the evaluation of current modeling approaches to the prediction and analysis of atmospheric release scenarios on the individual building scale. There were several stages of the experimental program: 1) characterization of the mean wind fields, 2) provision of averaged concentration measurements, 3) provision of high-resolution, transient wind and concentration data, and 4) provision of indoor concentration measurements concurrently with high-quality outdoor measurements on the individual building scale. A previous paper (Calhoun et al. 2004) has described in more detail stages 1 and 2. This paper is concerned primarily with stage 3.

   The rationale behind this paper is to begin to assess in a better way the contribution that the LES approach actually makes to modeling atmospheric releases. The experience of the authors has been that there are a number of particular challenges to performing an LES approach effectively. The first challenge is related to one of the strengths of LES—that transient signals can be easily and naturally produced. Therefore, most LES models will produce realistic-looking

transient signals. Because of the relative lack of high-resolution transient data for flows over individual buildings, one is tempted to believe that the individual vortices and fluid mechanical details seen in the LES fields are close to real, that is, that they are approximately accurate in time and space.

Second, the LES approach degrades (apparently) gracefully as the resolution of the grids decreases. Even though typical formulations of LES expect that the subgrid scale should begin in the inertial subrange of the turbulent cascade, realistic-looking results (though perhaps different) may still be obtained with poor grid resolution. Therefore, it is possible to operate an LES model with the subgrid-scale model performing essentially as a RANS turbulence model; that is, the effects of most of the energy-containing eddies are not resolved but rather are parameterized with the subgrid-scale model. To complicate the issue further, even an attempt to resolve in an honest manner the energy-containing eddies in the main flow field will usually break down near the walls, because the energy-containing eddies decrease in size as the wall is approached. There are current attempts to clarify the proper roles of RANS and LES near walls and to create a hybrid approach [see literature on detached-eddy simulation—e.g., Travin et al. (2000), or Squires et al. (2001)].

These challenges make the need for more detailed analysis of LES transient signals more pressing, especially because of advances in computer power and modeling methods that will tend to make the LES approach more popular.

One might legitimately ask why, in addition to a statistical description, we explore the degree to which transient signals are similar between the simulation and the measurements. Although these flows are turbulent and hence display chaotic behavior in detail, the LES method might allow us to focus on the larger scales of motion and treat the smallest scales statistically through the use of the subfilter-scale model. Hence, it is not inconceivable that the major portion of a signal describing a large vortex entering our flow domain might maintain some level of predictability across the domain. An increasing availability of real-time wind velocity information motivates our inquiry. For buildings that are important to a country's national security, arranging for real-time wind velocity information is relatively easy. The question becomes the following: Given real-time knowledge of wind direction shifts and variations in magnitude, can we improve modeling of flow and dispersion around buildings? Of course, in a mean sense, larger variations in wind direction can be related to larger horizontal eddy diffusivities. However, can, for example, an LES simulation capture a puff of airborne material that shifts to the other side of a building because of a 10-s shift in wind direction from 180° to 210°? Animations of LES fields would seem to indicate that it might be theoretically possible with this method. Many questions remain. For example, how much detail is required on the upwind flow boundary to allow an LES to capture some of these effects? Even if a real correlation between instantaneous velocities of the LES and measurements cannot be demonstrated, can the approximate movement of larger puffs of gas be simulated with a useful degree of accuracy? We begin to explore these questions below.

Model setup and numerical method

Model setup

As described in Calhoun et al. (2004), an architecturally complex building was chosen as the site of the field experiment. In contrast to results presented in Calhoun et al. (2004), however, this paper concerns only the final experimental day, 22 July 2000. This date was an intensive observation day with high-speed wind stations, "blue box" samplers [sulfur hexafluoride (SF_6) balloon sample boxes], and a Foxboro, Inc., Miran SF_6 real-time sampler.

Several important aspects of the simulation parameters are listed below [some of these aspects are similar to the aspects described in Calhoun et al. (2004), but others differ]:

1. The flow was assumed to be neutral and no heat flux was imposed at the ground, representing cloudy, morning, or higher wind conditions. As a consequence, only the experimental data that also represented neutral flow conditions were used in the following comparisons. The time of the year and conditions of the experiment were chosen so that neutral flow scenarios dominated for most of the duration of the experiment. Richardson number was used to determine if the flow was neutral based on an upwind sonic and energy budget station. This criterion typically requires strong winds such as existed on 22 July 2000 at the experimental site.

2. Canopy effects (trees) were modeled with the addition of a drag term in the momentum equations. Both ornamental trees and a large row of eucalyptus trees are modeled (see Fig. 18, described below). We follow, for example, Yamada (1982) and add the following term to the mean momentum equations:

$$\text{canopy\_drag} = \eta C_d a(z) U |U|, \qquad (1)$$

where η is the fraction covered by the canopy, C_d is the drag coefficient for the trees, $a(z)$ is the plant area density, and U is the x component of mean wind speed. An analogous term is used in the y direction. Because of the desire to keep the subfilter-scale turbulence model simple, no enhancement of the subfilter turbulence caused by the trees was implemented. Larger-scale enhancements to turbulence that could be resolved are naturally captured in the LES method. A standard value for the drag coefficient was taken from the literature (Yamada 1982).

3. Wind directions were generally from the southwest of the building. Precise wind directions upstream of the building were acquired with a high-speed sonic anemometer station. These speeds and wind directions were used to create an inflow profile (fitted to a logarithmic law), which was then used as input to the LES model. Incoming wind directions and speeds were updated every 1 s from the sonic anemometer data.

4. Approximately 2.85×10^6 grid points were utilized for the LES study. A fitted grid conforms precisely to the building shape. Marking some elements as belonging to a solid and others as being in the fluid [easily done in the finite-element method (FEM)] prevented undue deformation in the grid. Stretching allowed the finest grid resolutions near the building to be approximately 40 cm. The computational domain spans 600 m × 500 m × 80 m, where the smaller dimension is in the vertical direction. (Building height is about 10 m on average, but about five different vertical levels exist.)

5. A Smagorinsky subgrid-scale turbulence closure was used. The Smagorinsky coefficient was set to 0.2, and the length scale was set to the cube root of the volume of the computational cells. The authors have experience utilizing the dynamic eddy viscosity model based on the Germano identity (Calhoun and Street 2001), but it was

decided to use the simplest LES turbulence model for the simulations presented here. However, it would be interesting to consider carefully the role of the subgrid-scale model in building-type atmospheric flows (Tong et al. 1999).

6. Approximately 10 min of the study were simulated. The first 2 min of the model run simulated the 2 min before the release at 1830 Pacific daylight time (PDT), and the final 8 min simulated the first 8 min of the release. Assuming an approximate speed of 5 m s^{-1} across a domain 500 m across, the approximate number of flow-through times (the time for a fluid parcel to travel from inflow to outflow) simulated was six. Based on the authors' experience with channel flows, this sampling might be expected to yield converged values for low-order statistics. A longer simulation time would naturally be preferable, but cost was a consideration in these numerically intensive calculations.

7. The boundary conditions for the simulation were as follows. An inflow boundary was used upstream of the building and was formed by taking two levels of the velocity as measured by the sonic tower and fitting a logarithmic profile. An outflow boundary condition imposing zero gradient on the flow variables was used downstream. Outflow boundary conditions can have an effect upon the upstream flow near the outflow boundary (e.g., Sani and Gresho 1994). To quantify this effect properly, a series of simulations could be performed in which the outflow boundary is gradually moved downstream. Because these were expensive calculations, we used just two grids, one with a 400 m × 400 m × 80 m domain and a larger grid with a more distant downstream boundary (600 m × 500 m × 80 m). Moving the outflow boundary condition downstream avoided difficulties associated with large eddies forming near the edge of the trees that occasionally caused backflow conditions near the boundary. The upper boundary condition was free slip. On the lower boundary and building, the LES used a wall-layer model dependent on distance to the wall. The roughness of the building surface was assumed to be similar to that of concrete.

Summary of numerical method

The FEM used to solve the fluid dynamics was described briefly in Calhoun et al. (2004) and in detail in Chan (1994) and Gresho and Chan (1998). The code used was developed at the Lawrence Livermore National Laboratory (LLNL) and is a modern computational fluid dynamics code for solving the time-dependent Navier–Stokes equations through a combination of the finite-element method and a second-order projection method. The Poisson equation is solved with the multigrid method using software that is available through LLNL's Center for Applied Scientific Computing. Time stepping uses a semi-implicit projection method that is second-order accurate. An advantage of the FEM approach is its inherent capability, through the isoparametric element method, of performing simulations with complex geometry. For example, complex buildings can be naturally represented with the FEM approach.

The code was adapted for use on massively parallel computer platforms (Stevens et al. 2000) through the message passing interface. The modeling framework is an object-oriented approach. It was originally developed for applications using the adaptive-mesh-refinement technique. It was modified to perform well on distributed-memory computers while allowing the use of multiple dynamics drivers to customize the model to the problem of interest.

The simulations performed here used 256 processors of the Accelerated Strategic Computing Initiative "ASCI White" computer at LLNL. The computational domain spans 600 m × 500 m × 80 m, which is a larger domain in the x and y directions (extensions to the east and north on the aerial photo) than that of the RANS simulations of Calhoun et al. (2004). Large eddies advecting downstream made the outflow boundary condition unstable at shorter domain lengths.

Tracer experiment

The mean wind fields around the building and an evaluation of a RANS computer model to simulate these fields were conducted in the summer of 1999 and presented in Calhoun et al. (2004). In the summer of 2000, a set of releases of an inert and almost neutrally buoyant gas (SF_6) was conducted around the building. Large-eddy simulations were performed for the release experiment and are presented below. Figures 1 and 2 show photos of the experiment. In Fig. 2, the sonic anemometers can be seen mounted on tripods in the background. Notice the ornamental trees that complicate the flow scenario and the complex facade of the building seen in Fig. 1. A smoke generator was used to gain visual insight into the dispersal patterns around the building (Fig. 2).

Two types of samplers worked well in these experiments, a fast-response SF_6 sampler (Miran infrared spectrophotometer), and bag samplers (blue boxes), which collected air into Mylar bags at preprogrammed intervals. Bag samples were processed by mass spectrometry after the experiment. The Miran instrument provides real-time, fast-response SF_6 measurements. Data were sampled at 1-s intervals, and databases are available for running 5-s averages for most of the experiments. However, for the 22 July experiment 1-s data resolution is retained in the database. After appropriate averaging, the two types of SF_6 measurements have been shown to compare quite well in a subsequent experiment in Salt Lake City, Utah, in October of 2000 (Gouveia and Shinn 2002).

Releases were conducted in the following manner. The smoke generator and data from the sonic anemometers were used to help to find a good location for the source. Then, SF_6 gas was released at some recorded and fixed rate (in the range of 2–18 g s^{-1}) over the durations given (see Table 2, described below). A blower was used to mix the gas locally with a small volume of air as it was released. A summary of the experiments is provided in Table 1. Note (see Fig. 4, described below) that 22 July was an intensive measurement day with both the Miran sampler and nine box samplers—each with seven bags. The filling of the bags was controlled by synchronized on-box microprocessors and proceeded according to the schedule in Table 1.

Several comments may be of use to the reader who wishes to extend or corroborate the work presented here. First, because of the way that the sample boxes operate, that is, with 30 s of purging before filling the balloons, the actual start time of the balloon sample is 30 s after the times listed above. The balloons were filled in 10 s and then closed. Second, although the data are not presented in this paper, bag samples were also collected inside the building to understand better how gases may penetrate the building shell and ventilation systems. For the inside sample boxes, the 6th and 7th bags were filled at later times, in anticipation that the building would "store" SF_6 even after outside levels were very low. Interested readers should contact the authors to access the data. Data from the energy budget station showed that, for our

conditions, the wind speed was strong enough for shear forces to dominate buoyancy forces. Therefore the flow is treated as neutrally buoyant in the simulation.

Figure 3 is a summary map of all the release points, SF$_6$ sampling locations, and sonic anemometer stations. Figure 4 shows experimental setups for 22 July 2000. On 8 and 9 July 2000, the source was located off the southern and western corner of the building and the sampler was on the south side of the building. From Table 2, one can see that on 9 July there were a series of 3-min continuous point releases. The sampler seen in the map should be assumed to be the Miran sampler unless specified as being a blue-box sampler (bag sampler) on 22 July.

Experiment and data collection

Figure 4 [repeated from Calhoun et al. (2004) for convenience] shows the experimental setup on 22 July 2000. Each of the stations labeled "HS" is a sonic anemometer mounted on a tripod with a high-speed data acquisition system that records velocity data every 1 s. No on-box averaging was used at this time. Note that the HS tower upstream of the building contained two sonic anemometers at 4.4 and 8.8 m above the ground. The site marked "EB Station" refers to the energy budget station that was used to gather data on atmospheric stability. The Miran sampler also recorded data at the frequency of once per second. The blue-box samplers filled each of their seven Mylar balloons 30 s after the time listed for the bag number in Table 1. The heights of the instrumentation for the 22 July 2000 experiment are given in Table 3.

Model–experiment comparisons

Figure 5 illustrates several characteristics of the LES solution. An isosurface of concentration is shown, colored by wind speed. First, note the highly varying and transient solution. Animations of this and other views have been made by the authors. Second, notice how there are higher wind speeds, as should be expected, for the gap in the trees (higher speeds are represented by "warmer" colors; slow speeds are represented by "colder" colors). It also appears that this isosurface is pulled downward after passing through the line of eucalyptus trees.

Before looking at the high-frequency data, it is useful to view the 10-min-averaged data that are presented in Fig. 6. It is seen that HS stations 1, 2, and 5 all have much lower wind speeds, which clearly is caused by the fact that they are placed in recirculation zones, partially sheltered from the wind by the building. Between 1830 and 1840 PDT, the strongest winds are for HS station 7, which is located on top of the building. Wind directions, shown in Fig. 7, show a dramatic shift in direction for HS station 5, whereas the other stations appear to be much more stable. HS station 5 is in a location near the northwest corner of the building where gradients are strong and minor shifts in wind direction or position can mean the difference between being located in the recirculation behind the corner or in the free stream.

Upstream wind speed and direction for both the 4.4- and 8.8-m heights showed the expected increase in speed with height, and there did not appear to be systematic differences in wind direction between the two upstream heights—as one would expect in neutral conditions. The strongest winds during the experiment typically came from approximately 245°. Winds directly from the south are at 180° and winds from the west are at 270°. Therefore, the strongest winds are between these two, approximately out of the southwest, and, not coincidentally, aligned with the skewed direction of the north edge of the building. The building shields HS station 5 from the front when winds come from a more southerly direction, and blocks the flow from the back when winds are more northerly, creating a stagnation area with slower wind speeds.

Comparisons of high-frequency velocity signals

Comparisons between high-frequency signals of the velocity do not compare well everywhere. In particular, in the recirculation zones (HS stations 1 and 2), individual turbulent events do not compare well between the experiment and the simulation. However, HS station 7 compares somewhat more favorably (see Fig. 8). This may be because the original high correlation between the sonic anemometers and the inflow boundary condition has not traveled through any large wake or recirculation zones. These signals show, in general, a tendency of the model to have overly dramatic variances—an impression that is corroborated by statistical analysis in the next section. One might speculate that the eddy viscosity of the subgrid-scale model could be too low. The means appear to be reasonable in most of the signals, except for that of HS station 6 for which there is clearly both larger variances and too low an average magnitude for the *u* component of velocity. High-speed station 6 is located in a very challenging region to model correctly, that is, a high-gradient region that lies between the edge of a recirculation zone and outer, near-ambient-flow velocities. An error in location of either the numerical grid point or the sonic anemometer location will produce large errors in the signal.

Variances and covariances in the velocity signals

A statistical analysis, presented in Table 4, corroborates most of the impressions from a visual inspection of the signals. The means compare reasonably well for all stations except HS station 6 as explained above. The variances are systematically high for the model. Though some are better or worse, most variances compare within a factor of 2 or 3. In addition, the linear correlation coefficient is very low in the recirculation zones, indicating that the model cannot be considered predictive on an individual eddy-by-eddy basis. The linear correlation coefficient is defined as

$$r_{\text{LES-Sonic}} = \frac{\overline{(\text{LES})'(\text{Sonic})'}}{\sqrt{\overline{(\text{LES})'(\text{LES})'}}\ \sqrt{\overline{(\text{Sonic})'(\text{Sonic})'}}}.$$

Spectral analysis

Figures 9–11 plot frequency versus discrete spectral energy. From the spectral perspective, the comparisons appear to be reasonable, indicating that the model distributes energy among the various scales of eddy motions in a way that is roughly similar to that measured. In some cases, similar peaks in the spectrum appear when comparing model output versus measured data. For example, HS station 1 has peaks in both the sonic anemometer and LES data of magnitude approximately 0.17 between 0.02 and 0.03 Hz. Though it is important to keep in mind the fundamental equivalency between signals in physical and spectral space, the spectral perspective would, nevertheless, seem to indicate that the approximate shape of the distributions can be reproduced by the model.

u, υ event plots

The *u, υ* event plots in Figs. 12–14 also indicate that some features of the turbulence resolved in the model appear to have important similarities with measured data. As demonstrated through the roughly symmetrical cloud of points distributed around the axes for HS stations 1 and 2, both the model and the sonic anemometers indicate that the turbulence has a more isotropic character at these locations. The skewness of the distributions for HS stations 5, 6, and 7 shows that the model is roughly capturing an aspect of the flow physics, that is, the type of anisotropy. For example, even though in Fig. 13a the *u, υ* events are not distributed densely enough around the origin, the type of anisotropy is clearly reproduced.

Autocorrelations

Autocorrelations in time, $\overline{u(t)'u(t + \tau)'}/\overline{(u'u')}$, have been calculated and are displayed in Figs. 15 and 16. The idea behind this calculation is to learn over what length of time a signal is correlated with itself, which provides a measure of the size (in terms of time) of the largest energy-containing eddies. The model produces similar behavior when compared with the measured signals. For example, in Figs. 15a and 15b, model and experimental data both show a drop of the correlation to 0 at approximately 7 s. In general, the signals decorrelate, roughly, with 10–20-s time shifts. This result is consistent with the spectral analysis, which showed the most energy from 0 to 0.05 Hz [0.05 cycles per second (cps) is equal to 20 s per cycle].

TKE

The 2D turbulent kinetic energy (TKE) plots shown in Fig. 17 suffer from discrepancies similar to those of the variances above: the model overestimates the TKE and produces overly dramatic swings in the signal. Of course, it is to be expected that problems producing high-quality variances would propagate to the TKE plots, because TKE is a function of the variances. Note that, TKE is traditionally defined as ($\overline{(u'u'} + \overline{v'v')}/2$.

The spatial distribution of 2D TKE can be seen in Fig. 18. (North is directly up in the graph. The vertical level of the graph is at 2.5 m above the ground.) Regions of high TKE exist in and directly downstream of both gaps in the row of trees to the east of the building. This is expected because there are higher velocities through the gaps. Notice, as well, that two other regions of high TKE are located on the north side. One is on the northwest corner, because the flow must turn around the building, and the other is north of the northeast corner. The drag effects of the ornamental trees that are north, south, and east of the building can be seen as slow/blue regions with a circular shape. The model predicts relatively high TKE on the northeast side of the inner courtyard and low TKE near the southeast corner.

Concentrations

Comparisons with the blue-box sampler data are shown in Figs. 19–24. Three items are plotted in these graphs: the LES concentration curve, circle symbols representing the blue-box data, and boxes representing appropriate averaging of the LES concentration data for comparisons with blue-box data. Notice that the concentration comparisons are very good. The model predicts near-zero concentrations in the same places and times that the samplers found near-zero concentrations. In Fig. 22, the averaged LES concentrations at about 320 s do measure that more SF_6 is present; however, the unaveraged LES concentration curve shows a very good match with the data. It is clear from the sharp spike in the LES concentration data that averaging a slightly earlier section of the signal would produce the near-zero level that is measured. Likewise, when the samplers measured more significant concentrations of SF_6, the model produces impressively similar levels. For example, in Figs. 23 and 24, the model accurately produces both the magnitude and timing of the measured spike in SF_6 (see 320 s in both plots). Note that no significant levels of SF_6 were measured by blue boxes 12, 18, and 23. At these locations, the model also predicts no significant levels of SF_6.

It is even more interesting to compare the SF_6 concentration measured by the Miran real-time sampler with the LES data (Fig. 25). The initial onset, the magnitude, and the duration of the initial peak of tracer gas are accurately simulated. The second and third peaks of SF_6 are also approximately correct in both timing and magnitude. After this point, there was an unfortunate gap in the Miran data caused by instrument problems.

Conclusions

The purpose of this paper was to assess the ability of an LES model to add useful insight for flow scenarios around single buildings. Detailed results have been presented that compare SF_6 sampler data, high-speed sonic anemometer data, and simulated data. The simulation clearly captured some aspects of the turbulence observed in the experiment: type of anisotropy, spectral characteristics, and length of time for signals to decorrelate. However, the model did not perform nearly as well in the calculation of variances. Often the mean values were acceptable, but the model produced exaggerated swings in the signal and has not shown high correlations between the measured and modeled wind speed signals. This behavior was particularly true for the recirculation zones in which all of the high-speed sonic anemometer stations were placed, with the exception of HS station 7, which was located on the roof. As a consequence, the TKE comparisons had similar discrepancies. Despite these limitations, however, simulated concentrations matched closely the measured concentrations. In particular, these results suggest that high-resolution computational fluid dynamics models hold promise for adding insight into the onset, strength, and duration of transient atmospheric releases for single- or multiple-building scenarios.

The following recommendations are suggested. First, it is clear that LES is a numerically expensive and complex option and may be easily misused. It has been shown (Calhoun et al. 2004) that RANS and Gaussian approaches yield useful results, perhaps more than commensurate with their level of effort. Therefore, more complex models should perhaps be used in more specialized circumstances, where the luxury of additional time and effort can be afforded. Still, the complex model does appear to add valuable insight, and the difficulty in the calculation of variances might be addressed with a more accurate subgrid-scale model. Also, evidence from this study suggests that correctly capturing detailed eddy evolution is, at the very least, extremely challenging with the boundary condition used here. More information is likely required on the inflowing turbulence before LES can be expected to yield higher correlations between experiment and simulation on an eddy-to-eddy basis. As is to be expected, statistical properties such as spectral energy density, spatial decorrelation lengths of eddies, and level of anisotropy are easier to capture than are transient signals. Does it make sense

to use a data stream from upstream sonic anemometers combined with LES-style modeling so as better to characterize transient aspects of flow and dispersion around buildings of high interest? Some evidence from the SF_6 experiment–model comparison given here suggests that, at least in the near field, there is some possibility of useful model results. It is clear that improved upstream information is a priority, as is research on how best to filter or extend upstream data to create an upstream boundary condition.

Second, field experiments would appear to be essential toward the goal of improving computational fluid dynamics approaches. As faster computers increasingly allow more complex modeling methods, it will become more important to understand boundary and initial conditions accurately. In the above study, for example, the varying inflow boundary created from real sonic anemometer data gave the LES a higher degree of realism. However, better boundary conditions should be explored, preferably by incorporating data streams that are rich in spatial as well as temporal information.

Third, real-time tracer samplers vastly improve the ability to evaluate complex models. The Miran sampler performed well in the experiment, and one might imagine a future test with multiple real-time samplers deployed not only in the front of the building but also in the recirculation zones.

Acknowledgments

REFERENCES

Brown, M. 2001. Multiscale modeling of air flow in Salt Lake City and the surrounding region. *Proc. ASCE Structures Congress*, Washington, D.C., ASCE, LA-UR-01-509. S·F·X

Calhoun, R. and R. Street. 2001. Turbulent flow over a wavy surface. Part 1: Neutral case. J. Geophys. Res. 106:9277–9293. [CrossRef] S·F·X

Calhoun, R., S. Chan, R. Lee, J. Leone, J. Shinn, and D. Stevens. 2004. Flow around a complex building: Comparisons between experiments and a Reynolds-averaged Navier–Stokes approach. J. Appl. Meteor. 43:696–710. [Abstract] S·F·X

Chan, S. 1994. An improved three-dimensional heavy-gas dispersion model: User's manual. Lawrence Livermore National Laboratory Rep. UCRL-MA-116567 Rev. 1, 88 pp. S·F·X

Ding, L., R. Calhoun, and R. Street. 2003. Numerical simulation of strongly stratified flow over a three-dimensional hill. Bound.-Layer Meteor. 107:81–114. [CrossRef] S·F·X

Gouveia, F. and J. Shinn. 2002. Dense network of near-field observations of building-canopy winds and tracer concentrations during the Urban 2000 Experiment. Preprints, *Fourth Symp. on the Urban Environment*, Norfolk, VA, Amer. Meteor. Soc., 180–181. S·F·X

Gresho, P. and S. Chan. 1998. Projection 2 goes turbulent—and fully implicit. J. Comp. Fluid Dyn. 9:249–272. [CrossRef] S·F·X

Lawson, R., S. Perry, and R. Thompson. 2000. Measurement of velocity and concentration fields in arrays of 2-dimensional and 3-dimensional buildings in a simulated neutrally-buoyant atmospheric boundary layer. U.S. Environmental Protection Agency FMF Internal Data Rep., 55 pp. S·F·X

Mason, P. 1994. Large-eddy simulation: A critical review of the technique. Quart. J. Roy. Meteor. Soc. 120:1–26. [CrossRef] S·F·X

Murakami, S. 1993. Comparison of various turbulence models applied to a bluff body. J. Wind Eng. Ind. Aerodyn. 46–47:21–36. [CrossRef] S·F·X

Ramsdell, J. and C. Fosmire. 1998. Estimating concentrations in plumes released in the vicinity of buildings: Model development. Atmos. Environ. 32:10,. 1663–1677. [CrossRef] S·F·X

Sani, R. and P. Gresho. 1994. Resume and remarks on the open boundary condition minisymposium. Int. J. Numer. Methods Fluids 18:983–1008. [CrossRef] S·F·X
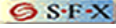
Snyder, W. 1994. Some observations of the influence of stratification on diffusion in building wakes. *Stably Stratified Flows: Flow and Dispersion over Topography,* I. P. Castro and N. J. Rockliff, Eds., Clarendon Press, 325–358. S·F·X

Squires, K., J. Forsythe, and P. Spalart. 2001. Detached-eddy simulation of the separated flow around a forebody cross-section. *Direct and Large-Eddy Simulation IV,* B. J. Geurts, R. Friedrich, and O. Metais, Eds., ERCOFTAC SeriesVol. 8, Kluwer Academic, 481–500. S·F·X

Stevens, D., A. Almgren, J. Bell, V. Beckner, and C. Rendleman. 2000. Small scale processes and entrainment in a stratocumulus marine boundary layer. J. Atmos. Sci. 57:567–581. [Abstract] S·F·X

Tong, C., J. Wyngaard, and J. Brasseur. 1999. Experimental study of the subgrid-scale stresses in the atmospheric surface layer. J. Atmos. Sci. 56:2277–2292. [Abstract] S·F·X

Travin, A., M. Shur, M. Strelets, and P. Spalart. 2000. Detached-eddy simulations past a circular cylinder. Flow Turb. Combust. 63:1-4,. 293–313. [CrossRef] S·F·X

Yamada, T. 1982. A numerical model study of turbulent airflow in and above a forest canopy. J. Meteor. Soc. Japan 60:439–454. S·F·X

FIG. 1.
North side of the building.

FIG. 2.
Side view of fogger release in front of the building.

FIG. 3.
Summary map for locations of releases, samplers, and anemometers.
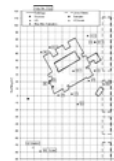
FIG. 4.
Instrument deployment map for 22 Jul; EB and HS are defined in the text and the Miran sampler is marked with a diamond at the SW corner of the building.
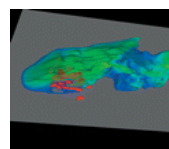
FIG. 5.
Simulated SF_6 release, depicting an isosurface of concentration colored by wind speed. Blue shades indicate slower wind speeds. Bright red (partially obscured) indicates buildings. Note that a row of eucalyptus trees is located to the east of the building (angling about 60° with respect to the horizontal plane)—compare this feature with Fig. 18, in which tree-induced retarded flow results in a blue region to the right of the building.

FIG. 6.
Ten-minute averages of wind speed for all HS stations, 22 Jul 2000.

FIG. 7.
Ten-minute averages of wind direction for all HS stations, 22 Jul 2000.

View larger version (50K)
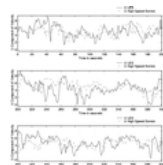
FIG. 8.
Simulated (solid line) vs measured (dot–dashed line) u component of velocity for HS station 7.

View larger version (58K)
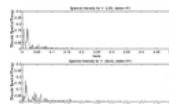
FIG. 9.
The (top) simulated vs (bottom) measured spectral intensity for v for HS station 1.

View larger version (34K)
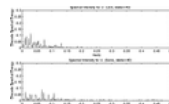
FIG. 10.
The (top) simulated vs (bottom) measured spectral intensity for u for HS station 2.

View larger version (34K)
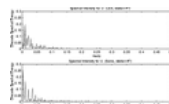
FIG. 11.
The (top) simulated vs (bottom) measured spectral intensity for u for HS station 7.

View larger version (34K)
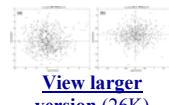
FIG. 12.
The (a) simulated and (b) measured u, v events for HS station 1.

View larger version (26K)
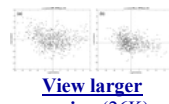
FIG. 13.
The (a) simulated and (b) measured u, v events for HS station 5.

View larger version (26K)
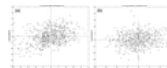
FIG. 14.

The (a) simulated and (b) measured u, v events for HS station 7.

View larger
version (27K)
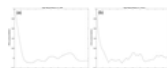
FIG. 15.

The (a) simulated and (b) measured autocorrelations of u in time at HS station 1.

View larger
version (16K)
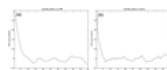
FIG. 16.

The (a) simulated and (b) measured autocorrelations of u in time at HS station 2.

View larger
version (17K)
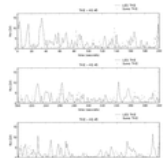
FIG. 17.

Simulated (solid line) vs measured (dot–dashed line) ($(\overline{u'u'} + \overline{v'v'})/2$ for HS station 5.

View larger
version (54K)
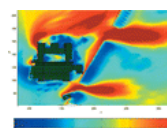
FIG. 18.

Simulated ($(\overline{u'u'} + \overline{v'v'})/2$. The vertical level of the horizontal plane depicted is 2.5 m above the ground. Note that the effect of the row of eucalyptus trees can be seen as the blue region angling to the right on the east side of the building.

View larger
version (102K)
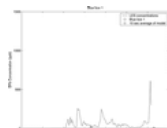
FIG. 19.

Simulated (solid line and squares) vs measured (circles) concentrations of SF_6 (ppb) for blue-box station 1.

View larger
version (27K)
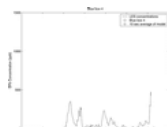
FIG. 20.

As in Fig. 19 but for blue-box station 4.

View larger
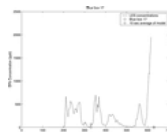
FIG. 21.
As in Fig. 19 but for blue-box station 17.
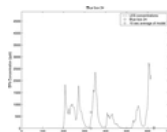
FIG. 22.
As in Fig. 19 but for blue-box station 24.
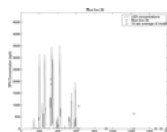
FIG. 23.
As in Fig. 19 but for blue-box station 39. Note that even though the simulation did not extend this long, a longer time is shown to demonstrate that this blue box measured a considerable amount of SF_6 at 1200 s.
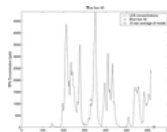
FIG. 24.
As in Fig. 19 but for blue-box station 45.
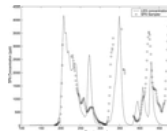
FIG. 25.
Concentrations of SF_6 (ppb) for real-time SF_6 sampler (circles) vs LES (solid line). The time range over which both sets of data are available is shown.

TABLE 1.
Sampling for outdoor blue boxes on 22 Jul 2000 (times are PDT).

TABLE 2.
Summary of releases of SF_6 in summer 2000.

View larger version (45K)

TABLE 3.
Heights of instruments for 22 Jul 2000.

View larger version (9K)

TABLE 4.
Statistical comparison of LES vs sonic anemometers for 22 Jul 2000.

View larger version (15K)

Cited by

Y.S. Liu, S.G. Miao, C.L. Zhang, G.X. Cui, Z.S. Zhang. (2012) Study on micro-atmospheric environment by coupling large eddy simulation with mesoscale model. *Journal of Wind Engineering and Industrial Aerodynamics* **107-108**, 106-117.
Online publication date: 1-Aug-2012.
CrossRef

Elie Bou-Zeid, Jan Overney, Benedict D. Rogers, Marc B. Parlange. (2009) The Effects of Building Representation and Clustering in Large-Eddy Simulations of Flows in Urban Canopies. *Boundary-Layer Meteorology* **132**:3, 415-436.
Online publication date: 1-Sep-2009.
CrossRef

Stevens T. Chan, Martin J. Leach. (2007) A Validation of FEM3MP with Joint Urban 2003 Data. *Journal of Applied Meteorology and Climatology* **46**:12, 2127-2146.
Online publication date: 1-Dec-2007.
Abstract . Full Text . PDF (3710 KB)

Julie K. Lundquist, Stevens T. Chan. (2007) Consequences of Urban Stability Conditions for Computational Fluid Dynamics Simulations of Urban Dispersion. *Journal of Applied Meteorology and Climatology* **46**:7, 1080-1097.
Online publication date: 1-Jul-2007.
Abstract . Full Text . PDF (1849 KB)

R. Calhoun, R. Heap, M. Princevac, R. Newsom, H. Fernando, D. Ligon. (2006) Virtual Towers Using Coherent Doppler Lidar during the Joint Urban 2003 Dispersion Experiment. *Journal of Applied Meteorology and Climatology* **45**:8, 1116-1126.
Online publication date: 1-Aug-2006.
Abstract . Full Text . PDF (1296 KB)